water

MDPI

Article

Thermal-Hydraulic Characteristics of the Liquid-Based Battery Thermal Management System with Intersected Serpentine Channels

Huaqiang Liu [1,*], Xiangcheng Gao [1], Dong Niu [1], Minghao Yu [1] and Yulong Ji [2,*]

[1] Department of Energy and Power Engineering, Naval Architecture and Ocean Engineering College, Dalian Maritime University, Dalian 116026, China
[2] Marine Engineering College, Dalian Maritime University, Dalian 116026, China
* Correspondence: huaqiang.liu@dlmu.edu.cn (H.L.); jiyulong@dlmu.edu.cn (Y.J.)

Abstract: Liquid thermal management is the prevailing method to maintain the operating performance and safety of Li-ion batteries. However, a better heat transfer performance is often accompanied by a higher power cost for liquid-based cooling methods. In the present work, V-shaped intersecting bypasses are integrated into conventional serpentine channels to reduce the liquid pressure drop across the cold plate without loss of thermal performance. The thermal-hydraulic characteristics of the battery thermal management system are studied based on CFD simulations. The non-dimensional j/f factor is developed and adopted to evaluate the heat transfer ability and friction loss of different designs. The effects of intersecting channel addition, flow direction, channel inlet, and outlet distributions are explored with the simulation results and data analysis. The results show that all of these factors would impact the thermal–hydraulic characteristics of the liquid cold plate. The addition of intersecting channels remarkably reduces the power cost, thus increasing the j/f factor. The alteration of the flow direction from longitudinal to widthwise could further improve the thermal-hydraulic characteristics of the intersected channel design. For conventional serpentine channels, the inlet and outlet distributions show no evident impact on thermal performance. However, regarding the intersected cases, the thermal-hydraulic performance is enhanced when the inlet and outlet are placed on the opposite sides of the cold plate, especially when the inlet velocity is less than 0.3 m/s. The findings of this study could shed light on the liquid flow channel design for battery thermal management.

Keywords: battery thermal management; liquid cold plate; serpentine flow channel; intersecting channels; thermal–hydraulic characteristics

Citation: Liu, H.; Gao, X.; Niu, D.; Yu, M.; Ji, Y. Thermal-Hydraulic Characteristics of the Liquid-Based Battery Thermal Management System with Intersected Serpentine Channels. *Water* **2022**, *14*, 3148. https://doi.org/10.3390/w14193148

Academic Editor: Dan Ma

Received: 27 August 2022
Accepted: 2 October 2022
Published: 6 October 2022

1. Introduction

Global warming originating from the ever-increasing greenhouse effect has become a significant concern all over the world. To combat climate change, the historic Paris Agreement was reached by almost all nations. It sets the goal of limiting the global temperature rise in this century well below 2 °C above pre-industrial levels [1], which imposes great pressure on the reduction of greenhouse gas emissions. According to statistical data, the transport sector is one of the main fossil fuel consumption markets, contributing largely to global greenhouse gas emissions [2]. As one of the key measures to realize the long-term temperature control objective, the intensity of carbon emissions from the transport sector needs to be dramatically reduced [3], which promotes the electrification of both vehicles [4] and vessels [5]. It was reported that, as of 2020, the number of electric vehicles all over the world had exceeded the magnitude of 10 million [6].

The lithium-ion (Li-ion) battery, which has the excellent characteristics of long cycling life, high energy density, low self-discharge loss, and high charge–discharge efficiency [7], is the dominant choice for power supply and energy storage [8]. The challenge is that, as

has been extensively reported in the literature, the operating performance and cycling life of Li-ion batteries are highly dependent on their working temperature [9]. The battery is expected to be kept within the temperature range of 25~40 °C [10]. Even worse, if the temperature exceeds the critical point, the irreversible thermal runaway process may occur, posing a threat to safety [11]. In addition, good temperature uniformity is supposed to be ensured to avoid local deterioration [12]. The battery temperature difference (that is, the difference between the maximum and minimum temperatures) must be kept below 5 °C [10]. Therefore, a battery thermal management system (BTMS) that effectively maintains the battery temperature is essential to ensure a long lifetime and avoid potential thermal runaway [13].

Existing BTMSs can be classified into air, liquid, heat pipe, and phase change material (PCM) cooling methods [14]. Despite the characteristics of low cost, lightweight, high design flexibility, and easy availability of cooling medium [15], the thermal efficiency of air cooling is rather poor and a large flow space is often required. Due to the high heat transfer performance, heat pipes are extensively employed for heat dissipation of high-heat-flux electronics. However, the integration issue of heat pipes into large battery packs at the pack level needs to be carefully evaluated and addressed before its wide practical application [16]. In addition, the manufacturing complexity and cost of the heat pipes are relatively high. PCM cooling is a promising thermal management method that could realize a high cooling capacity. Taking advantage of latent heat during the melting process from the solid phase to the liquid phase, the battery temperature could be effectively controlled around its melting points if a suitable PCM is chosen [17]. However, commonly used organic PCMs would suffer from the challenges of low thermal conductivity and potential leakage after melting [18]. In contrast, convective cooling with conductive liquid coolants is more suitable for harsh environments and high discharge rates, which demand high cooling efficiency [19]. The problem is that the circulation of the liquid coolant requires high pumping power consumption. To conclude, each battery thermal management method has its own pros and cons. By far, the liquid convective cooling approach is the prevalent choice for the thermal management of commercial electric vehicle batteries because of its strong heat transport capability and high reliability.

A frequently used form of liquid-based BTMS for prismatic batteries is to insert conductive cold plates with built-in coolant flow channels between battery cells. To meet the increasing demands for high battery power and fast discharging, the thermal performances of liquid-based BTMSs can generally be improved in two aspects, namely altering the thermo-physical properties of the cooling media and optimizing the flowing path structures. For example, the thermo-physical properties of the cooling media can be improved by dispersing nanoparticles [20]. Sarchami et al. [21] experimentally demonstrated that, compared to deionized water, the use of water-Al_2O_3 nanofluids could evidently decrease the battery's maximum temperature and improve the temperature uniformity. On the other hand, the heat transfer coefficient can be enhanced by optimizing the flow channel structures within the cold plates. For example, Jiang et al. [22] showed that the integration of V-shaped ribs with triangular cross sections could remarkably strengthen the heat transfer coefficient of straight flow channels. Liu et al. [23] demonstrated that alteration of straight liquid channels to helical channels could decrease the battery temperature.

However, improving battery thermal management performance with nanofluids and flow disturbing structures often implies a high pressure drop and a subsequent high pumping power cost [24], which is also an essential parameter that needs to be considered. It has been proven that a proper channel flow path design could dramatically reduce the viscous pressure drop [25]. The simulation results of Zuo et al. [26] illustrated that, with a double S channel design, the pumping power of the cold plate was reduced by 73.88%, and no evident loss of heat transfer performance was observed. Kong et al. [27] found that a cold plate with divergent channels could decrease both the pressure drop and the battery temperature difference than conventional straight channels.

To sum up, convective liquid cooling is an effective method to maintain the battery's temperature. However, the further improvement of liquid-based BTMSs is usually accompanied by the increment of pumping power consumption [28], which decreases the overall system efficiency in practical applications. Although there are some literature as mentioned above focusing on the flow channel improvement to reduce the pressure drop, the required pumping power still consumes a large amount of the battery power and needs to be eliminated. To address the problem of high friction cost, a novel serpentine channel design with V-shaped intersecting bypasses is proposed in the present work to improve the overall thermal-hydraulic characteristics of liquid-based cold plates for prismatic battery thermal management. The effects of intersecting channel addition, flow direction, and inlet and outlet distribution are investigated. The non-dimensional j/f factor is adopted to simultaneously evaluate the heat transfer performance and friction pressure drop of channel designs. It is expected that the conclusions achieved in the present study could shed light on the flow channel design for liquid cold plates.

The remainder of the paper is organized as follows. Section 2 depicts the physical model of the considered BTMS, while the governing equations, the simulation setups, and the data reduction methods are elaborated in Section 3. Section 4 presents the numerical results and thermal performance under different conditions. In the end, the research findings obtained in the present work are presented in the last section.

2. Physical Problem

In commercial electric vehicles, a battery pack is made up of several battery modules, each of which would consist of thousands of battery cells connected in series or parallel. For prismatic Li-ion batteries, cold plates with built-in coolant flow channels are normally adopted and placed between cells, as shown in Figure 1, to dissipate way the excessive heat generated by Li-ion batteries and maintain the battery temperature in the desired range. In the present work, an 8.0 Ah prismatic $LiFePO_4$ Li-ion battery with dimensions of 124 mm $\times$ 79 mm $\times$ 17 mm is studied [29]. Considering the symmetrical nature of the battery module, half of the domain is considered, as illustrated in Figure 1c, to investigate the system thermal performance. In addition, the configuration and geometrical parameters of the intersected serpentine channel are shown in Figure 1c. The thicknesses of the solid cold plate t_s and the flowing channel t_c are kept as 3 mm and 2 mm. The width of the main serpentine channel w_c is maintained at 3.5 mm. To improve the overall performance of the conventional serpentine channel cold plate, V-shaped intersecting channels are incorporated to decrease the pressure drop along the flowing channel. The influencing geometrical parameters of the intersecting channels are shown in Figure 1b, including the intersecting width w_{int}, the intersecting angle θ, and the intersecting distance d. Li-ion batteries are usually produced by stacking up anode, separator, and cathode layers. The detailed simulation of different battery sandwich layers would require massive computation costs. In the present study, to simplify the simulation model, the battery is assumed to be a simple block made of materials with uniform properties. Accessories such as current tabs, safety vents, and electrical wires are ignored. The thermo-physical properties of the materials used in the studied BTMS are summarized in Table 1.

In the present study, the performances of different serpentine flow channel designs within the cold plate are investigated and compared. The geometry schematics of the considered flow directions and intersecting channels are shown in Figure 2. As can be seen from the figure, Cases 1, 3, and 5 are conventional serpentine flow channels with different distribution patterns of flow inlet and outlet, while V-shaped intersected channels are incorporated in Cases 2, 4, and 6. Cases 1 and 2 are the channel designs with longitudinal flow direction and coolant flows in the widthwise direction for Cases 3–6. Apart from the flow direction, the impacts of the inlet and outlet distributions are also investigated. Different from the setup in Cases 1–4, the channel inlet and outlet are distributed on opposite sides of the cold plate. The detailed geometry parameters for these cases are given in Table 2. The dimensions of the main flow channel cross section are maintained

identically for all the cases, and the intersecting channel quantity is kept as 7 along the main flow direction. The width w_{int} and angle θ of all the intersecting channels are set as 2.0 mm and 45°, respectively.

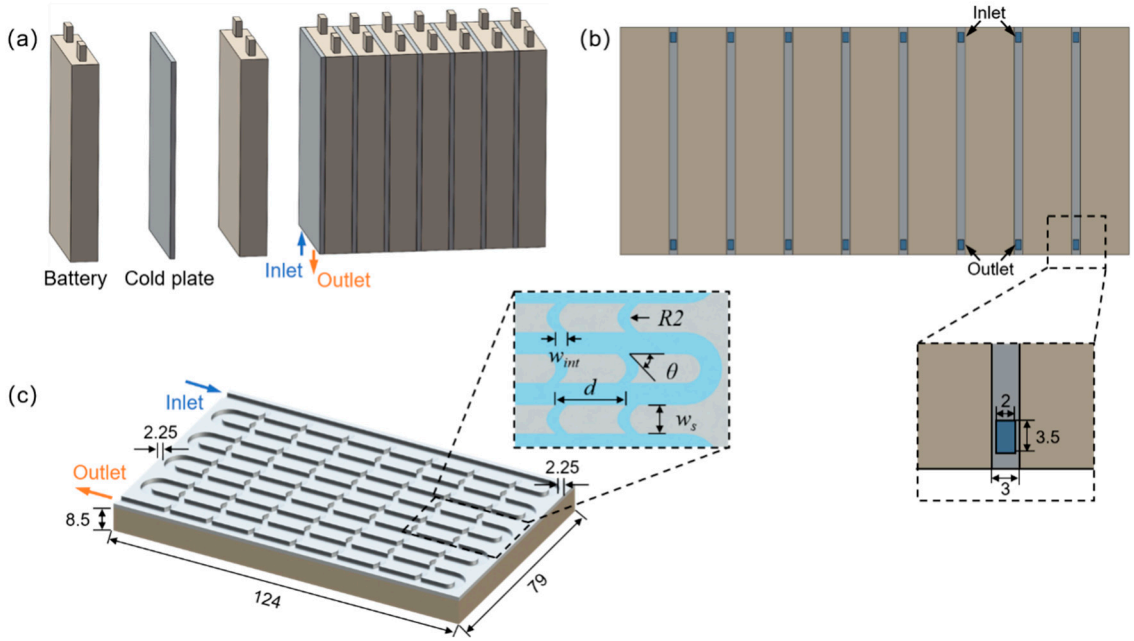

Figure 1. Schematics of the investigated battery thermal management system: (**a**) battery module; (**b**) bottom view; (**c**) simplified model with intersected serpentine flow channels (units: mm).

Table 1. Thermo-physical properties of the materials used in the present study.

Component	Density ($kg \cdot m^{-3}$)	Specific Heat Capacity ($J \cdot kg^{-1} \cdot K^{-1}$)	Thermal Conductivity ($W \cdot m^{-1} \cdot K^{-1}$)	Dynamic Viscosity ($kg \cdot m^{-1} \cdot s^{-1}$)
Battery	1969.6	1305	2.6	
Cold plate	2719	871	202.4	
Water	998	4200	0.6	0.001003

Table 2. Parameter values for the flow channels within the cold plate.

Case No.	w_{int} (mm)	θ (°)	D (mm)	w_s (mm)
1				4.5
2	2	45	15	4.5
3				5.5
4	2	45	8.5	5.5
5				3.7
6	2	45	8.5	3.7

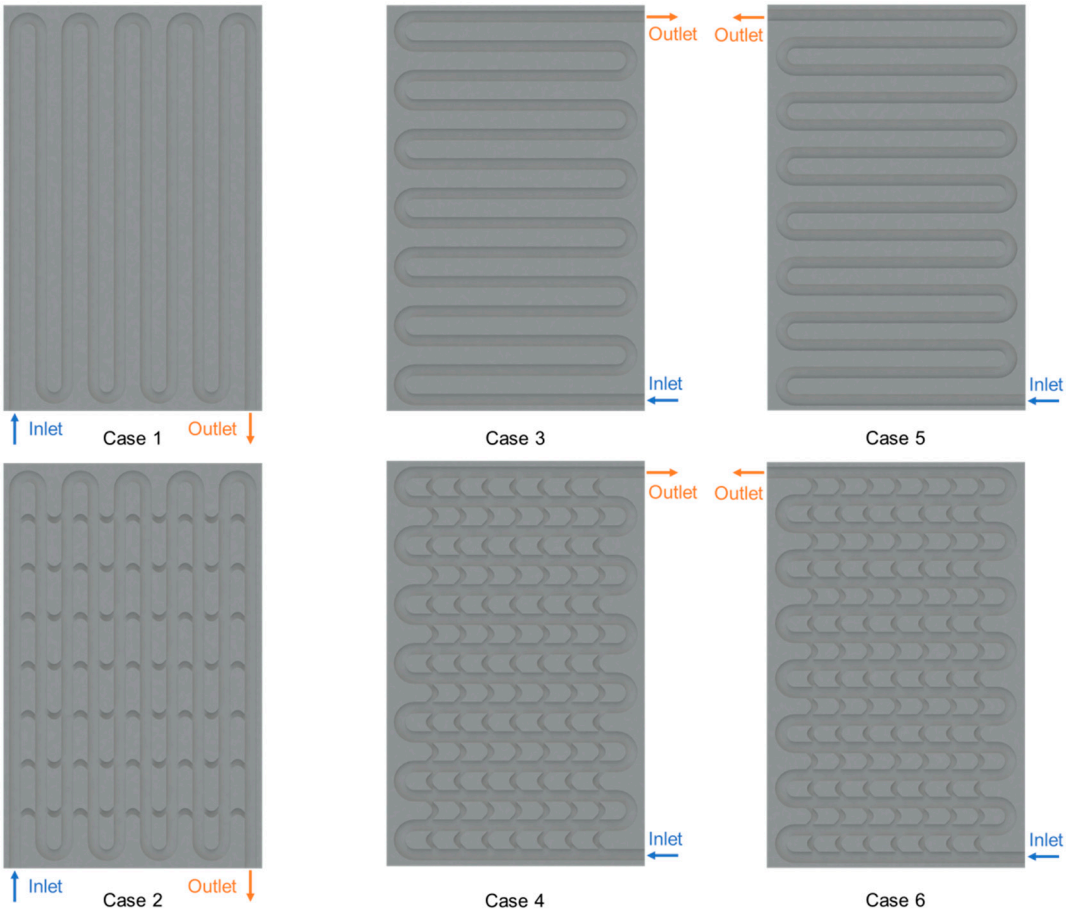

Figure 2. Schematics of the flow channel designs investigated in the present study. Cases 1, 3, and 5 are channel designs without intersecting branches while Cases 2, 4, and 6 are with V-shaped intersecting branches.

3. Numerical Methodology

3.1. Governing Equations

The energy conservation equation for the battery cell is given as

$$\rho_b C_{p,b} \frac{\partial T_b}{\partial t} = k_b \nabla^2 T_b + \dot{q}_{gen} \tag{1}$$

where ρ_b, $C_{p,b}$, k_b, and T_b are the battery density, specific heat capacity, thermal conductivity, and temperature, respectively. The heat source term, $\dot{q}_{gen}$, is the battery volumetric heat generation rate, which varies with the discharge rate (C-rate) and the state of charge (SOC).

In the present study, the polynomial heat generation rate expressions under different discharge rates from [29], which are derived by fitting the experimentally measured hybrid pulse power characterization data, are adopted and given as Equation (2). The fitted constants in the equation for different discharge rates are listed in Table 3.

$$\dot{q}_{gen} = k_0 + k_1 \cdot SOC + k_2 \cdot SOC^2 + k_3 \cdot SOC^3 + k_4 \cdot SOC^4 + k_5 \cdot SOC^5 + k_6 \cdot SOC^6 \tag{2}$$

$$SOC = 1 - It/C \tag{3}$$

where I is the discharge current and t is the discharge time. C is the nominal capacity of the battery.

Table 3. The constants in the battery heat generation rate fitted equations. Reproduced with permission from Elsevier [29].

$\dot{q}_{gen}$ (kW/m^3)	k_0	k_1	k_2	k_3	k_4	k_5	k_6
3C	41.0	−304.4	1659.1	−4680.6	6952.1	−5159.3	1508.1
5C	103.7	−974.8	5809.6	−16714.2	24662.9	−17955.2	5109.9
7C	217.1	−2328.3	14668.5	−44043.1	67368.9	−50759.4	14947.9
9C	319.6	−2719.0	15148.5	−43018.3	63645.5	−46817.9	13527.5

The fluid flow in the channels can be described by the continuity and momentum conservation equations as follows

$$\nabla \cdot \vec{v} = 0 \tag{4}$$

$$\rho_c \left[\frac{\partial \vec{v}}{\partial t} + \left(\vec{v} \cdot \nabla \right) \vec{v} \right] = -\nabla p + \mu \nabla^2 \vec{v} \tag{5}$$

where $\vec{v}$ is the fluid velocity vector; ρ_c is the fluid density; p and μ are the static pressure and dynamic viscosity of the coolant.

The energy conservation equation for the coolant is

$$\rho_c C_{p,c} \frac{\partial T_c}{\partial t} + \nabla \cdot \left(\rho_c C_{p,c} \vec{v} T_c \right) = \nabla \cdot (k_c \nabla T_c) \tag{6}$$

where $C_{p,c}$, k_c, and T_c are the specific heat capacity, thermal conductivity, and temperature of the cooling medium, respectively.

The energy conservation equation for the solid cold plate is given as

$$\rho_s C_{p,s} \frac{\partial T_s}{\partial t} = k_s \nabla^2 T_s \tag{7}$$

where ρ_s, $C_{p,s}$, k_s, and T_s are the density, specific heat capacity, thermal conductivity, and temperature of the solid cold plate, respectively.

3.2. Data Reduction

The battery temperature and the corresponding power cost are essential parameters that need to be considered for battery thermal management. For liquid-based BTMSs, it is expected that a proper battery temperature could be achieved at the expense of low required pumping power. The non-dimensional evaluation index, the j/f factor, is adopted to quantitatively assess the efficacy of the cold plate design in the present study. The Colburn j-factor and the fanning friction factor f are widely used to characterize the thermal–hydraulic performance of compact heat exchangers [30]. The Colburn j-factor is calculated by

$$j = \frac{Nu}{RePr^{1/3}} \tag{8}$$

where Nu is the Nusselt number, while Re and Pr represent the dimensionless Reynolds number and Prandtl number, respectively. The Prandtl number, Pr, is assumed to be constant, which is approximately 5.41 for water at 30 °C. Re, calculated by Equation (9), is related to the inlet flow velocity and the sizes of the flow channel cross-section.

$$Re = \rho_c u_{in} D_h / \mu \tag{9}$$

where ρ_c is the coolant density, and u_{in} is the inlet velocity; μ is the dynamic viscosity of the coolant; D_h represents the hydraulic diameter of the flow channel and is calculated by $D_h = 4A_{cs}/P_{cs}$. Here, A_{cs} and P_{cs} are the area and perimeter of the channel cross-section.

The expression of the Nusselt number is

$$Nu = hD_h/k_c \tag{10}$$

where h is the average heat transfer coefficient, which is calculated using Equation (11), and k_c is the coolant thermal conductivity.

$$h = \frac{\dot{Q}}{A_c\left[T_{ave} - T_f\right]} \tag{11}$$

Here, $\dot{Q}$ represents the energy transported away by the flowing coolant and its formula is given as Equation (12); A_c is the channel heat exchange area; T_{ave} is the average battery temperature; T_f is the bulk fluid temperature, which is assumed as the mean value of the fluid inlet and outlet temperatures, $(T_{out} + T_{in})/2$.

$$\dot{Q} = \dot{m}C_{p,c}(T_{out} - T_{in}) = \rho_c u_{in} A_{cs} C_{p,c}(T_{out} - T_{in}) \tag{12}$$

The formula for calculating the fanning friction factor is expressed as

$$f = \frac{\Delta p D_h}{2\rho_c {u_{in}}^2 L} \tag{13}$$

where Δp is the pressure drop within the channel, which is calculated to be the pressure difference between the channel inlet and outlet, that is, $p_{in} - p_{out}$, and L is the length of the flow channel.

Moreover, the required pumping power is calculated by

$$P = \dot{V}_{in}\Delta p = A_{cs} u_{in} \Delta p \tag{14}$$

where $\dot{V}_{in}$ is the volumetric flow rate.

The battery temperature difference is also a critical thermal management indicator that reflects the temperature uniformity within the battery cell. It is calculated to be the difference between the battery maximum and minimum temperature.

$$\Delta T = T_{max} - T_{min} \tag{15}$$

3.3. Numerical Details

The finite-volume method based CFD software, ANSYS Fluent, is adopted to numerically investigate the battery thermal management performance with different cold plat channel designs. Control equations are solved using the transient pressure-based segregated solver and SIMPLE scheme with second-order upwind spatial discretization. The conservation criteria for the continuity, momentum, and energy equations are set as 10^{-4}, 10^{-4}, and 10^{-6}, respectively. According to calculations, the maximum Reynolds number in the present study is less than 2300. Therefore, the laminar flow model is employed. The inlet coolant temperature is the same as the environment temperature (i.e., 30 °C), which is also the initial system temperature. The top and bottom surfaces of the simplified model are set as symmetry. The exterior surfaces of the cold plate and battery are subjected to a natural convection condition with the ambient and the convection coefficient is given as 5 $W{\cdot}m^{-2}{\cdot}K^{-1}$. The no-slip boundary condition is applied for the flow channel interior walls.

The SOC-dependent battery heat generation is incorporated using self-written user-defined functions. The experimentally measured battery temperature evolution and the simulation results during the discharge process at different C-rates without thermal management systems are presented in Figure 3. It is shown that the simulation results obtained in this study agreed well with the experimental data of [29] at different discharge rates,

which proves the efficacy of the battery heat generation equations and the employed simulation model.

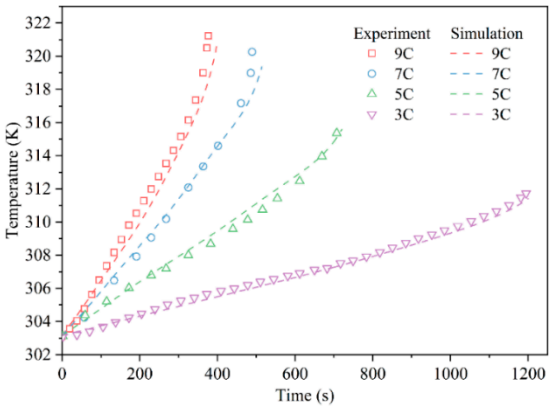

Figure 3. The battery temperature variations from simulation results and experimental data. Reproduced with permission from Elsevier [29].

Prior to the simulations for different cases, the mesh sensitivity check is performed to determine the appropriate mesh size. Taking the V-shaped intersecting design shown in Figure 1 as an example, grids with elements ranging from 1,173,306 to 2,334,351 are employed to simulate the battery temperature variations under 9C discharge. The inlet flow velocity is maintained at 0.2 m/s. The corresponding battery maximum temperatures are shown in Figure 4a and there is negligible difference reported for the simulation results with different mesh sizes. Additionally, timesteps of 0.5, 1.0, and 2.0 s were utilized to check the timestep independence. Similarly, no obvious discrepancy was observed for cases with different timesteps in the studied range. Taking into account both the accuracy and the simulation cost, the grid with an element number of 1,770,592 and a timestep of 1.0 s was adopted in the present work.

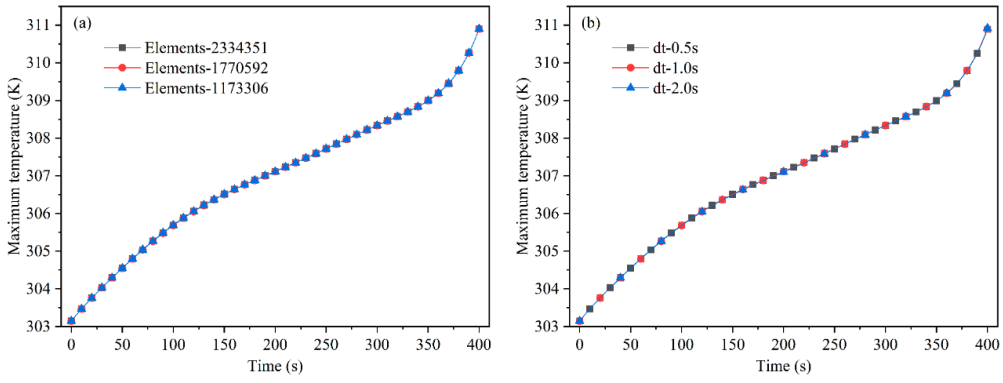

Figure 4. (**a**) Mesh sensitivity check; (**b**) Timestep sensitivity check.

The experimentally measured temperature data of a serpentine heat sink [31] are compared with the simulation results obtained using the present numerical methods to further demonstrate the validity of the simulation model. The configuration of the heat sink is shown in Figure 5a, which is similar to the cold plate with the conventional serpentine channel investigated in this study. The simulation conditions, which can be found in [31], are maintained the same as those in the original experiment. The base temperature comparison between the experimental and simulation results is shown in Figure 5b. It is seen that a good agreement between the base temperature variations obtained using the simulation model and the experimentally measured data with varying mass flow rates is achieved, manifesting the validity of the numerical model in present study.

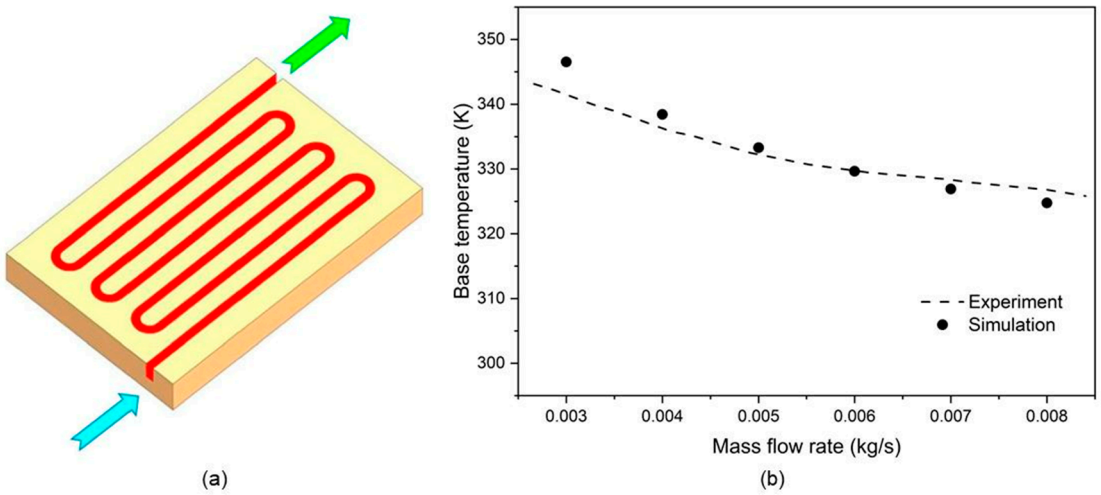

Figure 5. Simulation model validation with experimental results of serpentine heat sink from [31]: (**a**) Serpentine heat sink configuration; (**b**) Base temperature comparison. Reproduced with permission from Elsevier [31].

4. Results

In the present study, the thermal performances of several flow channel designs for prismatic Li-ion battery thermal management are studied. Specifically, the effects of the main flow direction, the addition of intersecting channels, and the inlet and outlet distribution are examined. During the simulations, the cooling medium enters the channel inlet with a constant flow velocity.

4.1. Effects of Flow Direction and Intersecting Channels

To demonstrate the effects of flow direction and the addition of intersecting channels, the thermal performances of the serpentine channel designs of Cases 1–4 at the end of 9C discharge process are shown in Figure 6. As elucidated in Figure 2, the coolant flows along the longitudinal direction in Cases 1 and 2 while it is in the widthwise direction for Cases 3 and 4. The results demonstrate that, compared to Cases 2 and 4 with integrated intersecting channels, Cases 3 and 4 achieve better performance in terms of maximum battery temperature at a given inlet velocity, especially when the flow velocity is smaller than 0.4 m/s. However, the intersected design with a widthwise flow direction (i.e., Case 4) has superior performance at high inlet velocities, which realized the lowest T_{max} at the inlet velocity of 0.5 m/s. Comparatively, the poorest performance is observed for Case 1 within the entire studied range in terms of maximum temperature. The variation trends for the battery temperature difference are similar to those of the maximum temperature. It is reasonable since the temperature difference is the deviation between the maximum temperature and minimum temperature, and because of the fixed inlet temperature and velocity of the coolant, the minimum battery temperatures for different cases are close.

As for the average battery temperature as shown in Figure 6b, the cases with widthwise flow direction present a better performance at a given inlet velocity, and the addition of intersecting channels further reduces the average temperature. The intersected serpentine channel with longitudinal flow direction performs the poorest at the velocity of less than 0.2 m/s, but its performance becomes better at high inlet flow speeds and gradually exceeds that of Case 3. The difference between the average temperatures for those cases are mainly originated from the interfacial solid–liquid area, which determines the heat transfer surface size. The addition of intersecting channels apparently increases the heat transfer surface area.

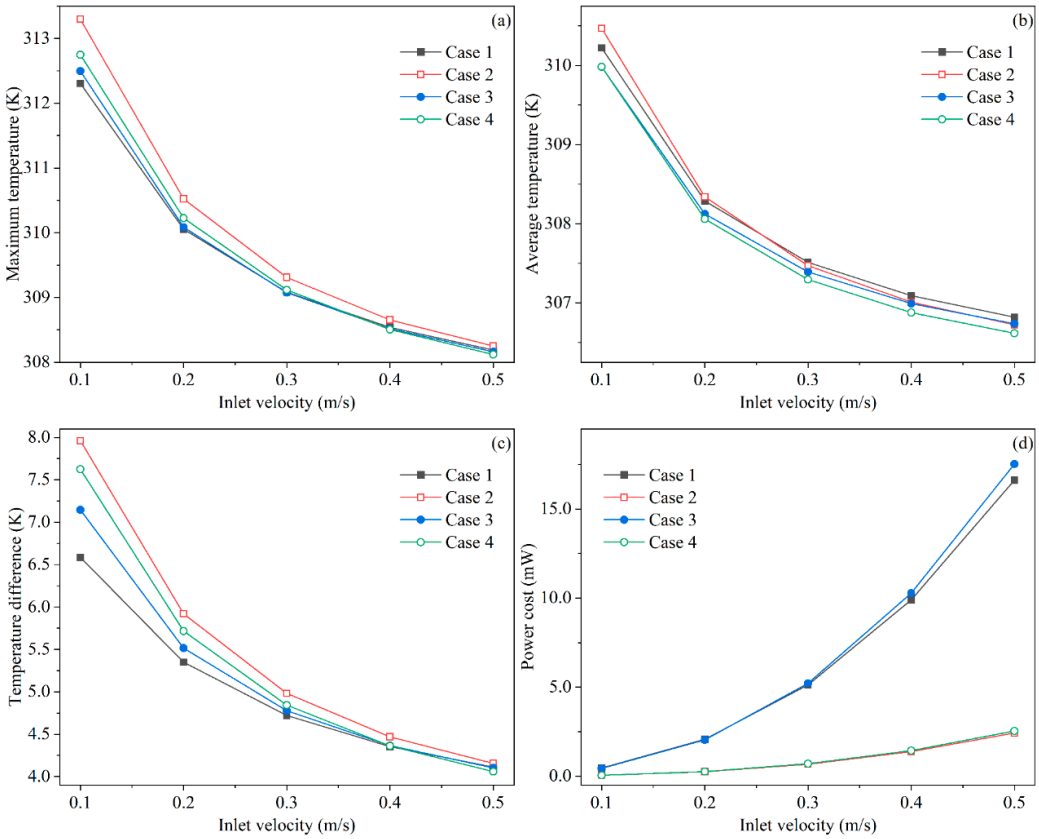

Figure 6. Thermal-hydraulic performance of Cases 1–4 with the variation of inlet flow velocity: (**a**) maximum battery temperature; (**b**) average battery temperature; (**c**) battery temperature difference, and (**d**) required power cost.

The power cost required for fluid circulation in the flow channel, which increases markedly with the increasing inlet velocity, exhibits a somewhat different variation trend from the battery temperature evolution. Compared to the widthwise flow cases, the power cost is lower when the main flow direction is longitudinal, although only a slight discrepancy is observed. It is also observed that compared to the conventional serpentine designs, the incorporated intersecting channels could remarkably decrease power consumption. Among these cases, the power cost of Case 2 is the lowest, which is 2.43 mW at the inlet velocity of 0.5 m/s while it becomes 17.5 mW for Case 3 under the same working condition. The cause of the evident pressure drop reduction brought by the addition of intersecting channels will be explained next.

To better depict the effects of flow direction and intersecting channel design on the thermal-hydraulic characteristics of the cold plate, the temperature distribution across the central battery surface and the pressure field within the central surface of the fluid channel for different channel designs at an inlet velocity of 0.2 m/s are shown in Figure 7. In general, the battery temperature near the channel inlet is close to the ambient temperature, and a high-temperature region is observed near the outlet for all the cases. This is because the incoming coolant has a strong heat-absorbing capability due to the low fluid temperature near the channel inlet, but as the fluid temperature gradually increases along the flow channel, the temperature difference between the battery and the cooling medium is narrowed, resulting in a weakened cooling ability. For conventional serpentine channel cases, there exist two local cold spots which are located at the inlet area and the first channel bend, respectively. The addition of intersecting channels expands the cold region near the inlet and shifts the hot spot to the catty-corner from the inlet. This is because the bypass channels divide the main flow into branches. A large amount of coolant flows toward the outlet without passing by the other end of the cold plate, thus weakening the coolant

cooling capability at the catty-corner from the inlet which is demonstrated by the pathlines in Figure 8. This also leads to the higher battery maximum temperature and temperature difference for Cases 2 and 4.

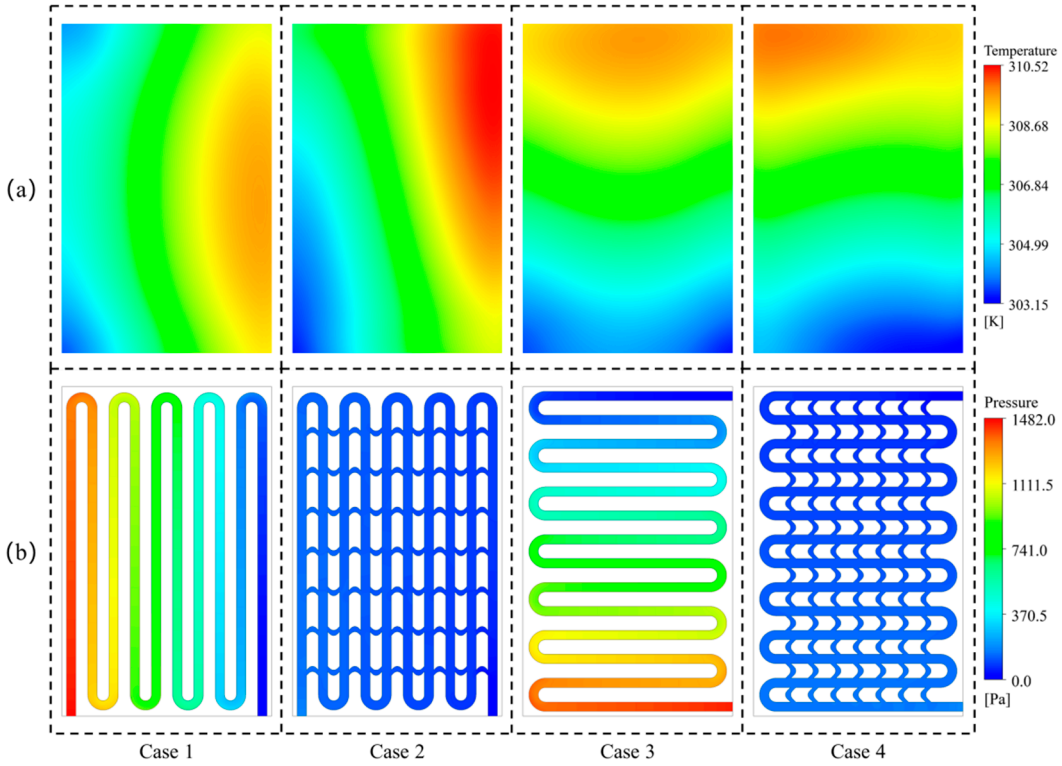

Figure 7. Thermal performances of different channel designs: (**a**) temperature contours across the battery central surface; (**b**) pressure contours of the channel central surface.

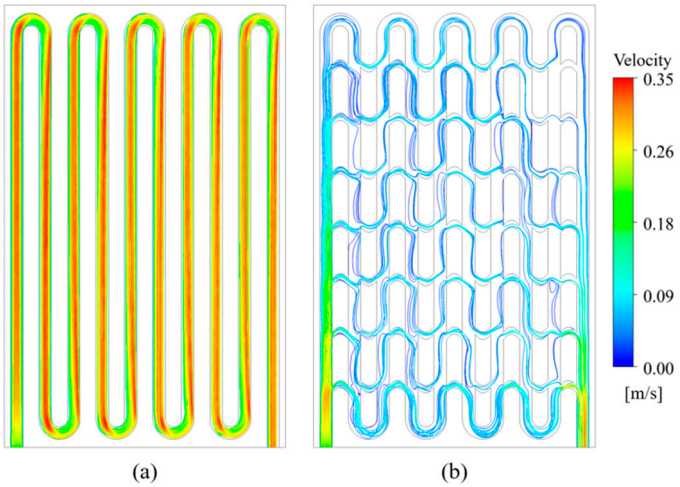

Figure 8. Pathlines for the (**a**) conventional serpentine channel and (**b**) the intersected channel at the inlet velocity of 0.2 m/s.

As shown in Figure 7b, compared to the pressure profiles for Cases 1 and 3, the pressure inside the intersected channels is negligible. Due to the fixed pressure at the channel outlet, the higher pressure at the inlet area indicates the higher pressure drop across the entire flow channel for conventional serpentine channel designs. It occurs because the evenly distributed bypasses are able to separate the main stream in the serpentine channel into branches and reduce the average flow speed, as can be seen in Figure 8. Moreover,

the coolant experiences a large velocity change with the flow direction reversion at the serpentine channel turn, which increases the pressure loss along the flow path. On the other hand, a large portion of fluid would flow toward the outlet through the bifurcated channels. The length of the corresponding flow path is shorter than that of the main serpentine channel, which could also decrease the friction loss.

It is well-known that pressure drop is directly dependent on the flow distance. It seems that the addition of intersected channels would increase the channel length and the viscous pressure drop. However, as mentioned above, the integrated intersected channels dramatically decrease the pressure drop instead. To explain the effects brought by the V-shaped intersected channels, the streamlines with 150 sampling points for the conventional serpentine channel and the intersected channel at the inlet velocity of 0.2 m/s are given in Figure 8. It is clearly seen that for the conventional serpentine channel case, the coolant needs to flow through the whole channel to reach the outlet region, while for the intersected channel case, the integrated V-shaped channels divided the mainstream into branches, and the coolant is relatively uniformly distributed in the bypasses. Therefore, the total flow length for the conventional serpentine channel is the length of the whole channel, while it is the length of the V-shaped bypasses for the intersected case, the maximum of which is much smaller than the whole serpentine channel. This is why the integration of V-shaped bypasses could dramatically reduce the pressure drop, although it seems that a longer channel length is introduced which is not the fact for the coolant flow.

To evaluate the heat transfer performance and friction loss simultaneously for different channel designs, the non-dimensional *j/f* factor variations with the inlet velocity are calculated and demonstrated in Figure 9. A larger *j/f* factor manifests a higher cooling efficiency at the expense of the given viscous loss. In general, the *j/f* factor is enlarged with increasing velocity, although it starts to decline slightly beyond the velocity of 0.3 m/s for Cases 2 and 4. It denotes the relatively higher cooling efficiency under high flow velocities. Moreover, it is found that the bifurcating channels of Cases 2 and 4 could significantly enhance the thermal-hydraulic performance. The *j/f* factor for Case 3 is 0.089 at the velocity of 0.3 m/s while the addition of intersecting channels promotes the magnitude to 0.674. The effect of the flow direction is not unified. For conventional serpentine cases, the *j/f* factor is higher when the flow direction is longitudinal, but it is remarkably higher in the widthwise flow direction when intersected channels are considered.

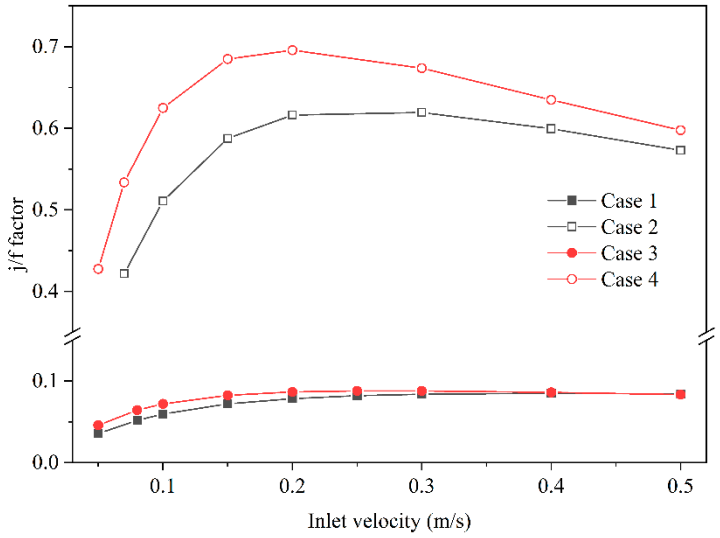

Figure 9. Variations of the *j/f* factor with the inlet velocity change for Cases 1–4.

4.2. Effects of Inlet and Outlet Distribution

The thermal–hydraulic characteristics of Cases 3–6 along with the inlet flow velocity are shown in Figure 10 to demonstrate the effect of the channel inlet and outlet distribution. The inlet and outlet are placed on the same side of the cold plate in Cases 3 and 4 while in

Cases 5 and 6, they are on the opposite sides. From the perspective of maximum temperature, Case 4 presents a relatively poor performance in low velocity, but the discrepancy is narrowed with the increment of inlet velocity. When the velocity exceeds 0.4 m/s, the battery maximum temperature for Case 4 becomes the lowest among the studied cases. The maximum temperatures for the other designs show a negligible difference within the studied velocity range. The reduction of the maximum temperature from Case 4 to Case 6 at low inlet velocities is because the alteration of the outlet position could eliminate the coolant shortage problem at the catty-corner from the inlet which results from the intersecting channel addition. The battery average temperature presents a different variation trend. At the velocity of 0.1 m/s, the average temperature remains around 310 K for all these cases, but as the velocity increases, the discrepancy becomes larger. The intersected channel designs of Cases 4 and 6 achieved lower T_{ave} than the conventional serpentine designs because of the enlarged heat transfer surfaces. Regarding the battery temperature difference, Case 3 achieved the best performance, followed by Case 3, 6, and 4 with low inlet velocities. However, the performance of Case 4 improves quickly with the velocity growth and surpasses the other channel designs when the velocity is beyond 0.4 m/s. The required pumping powers for these channel designs are presented in Figure 10d. Remarkably, the addition of intersecting channels dramatically decreases the power cost. Designs with opposite channel openings (Case 5 and 6) have higher power consumption than the same side designs (Case 3 and 4), which is caused by the relatively longer flow path and, subsequently, higher friction loss.

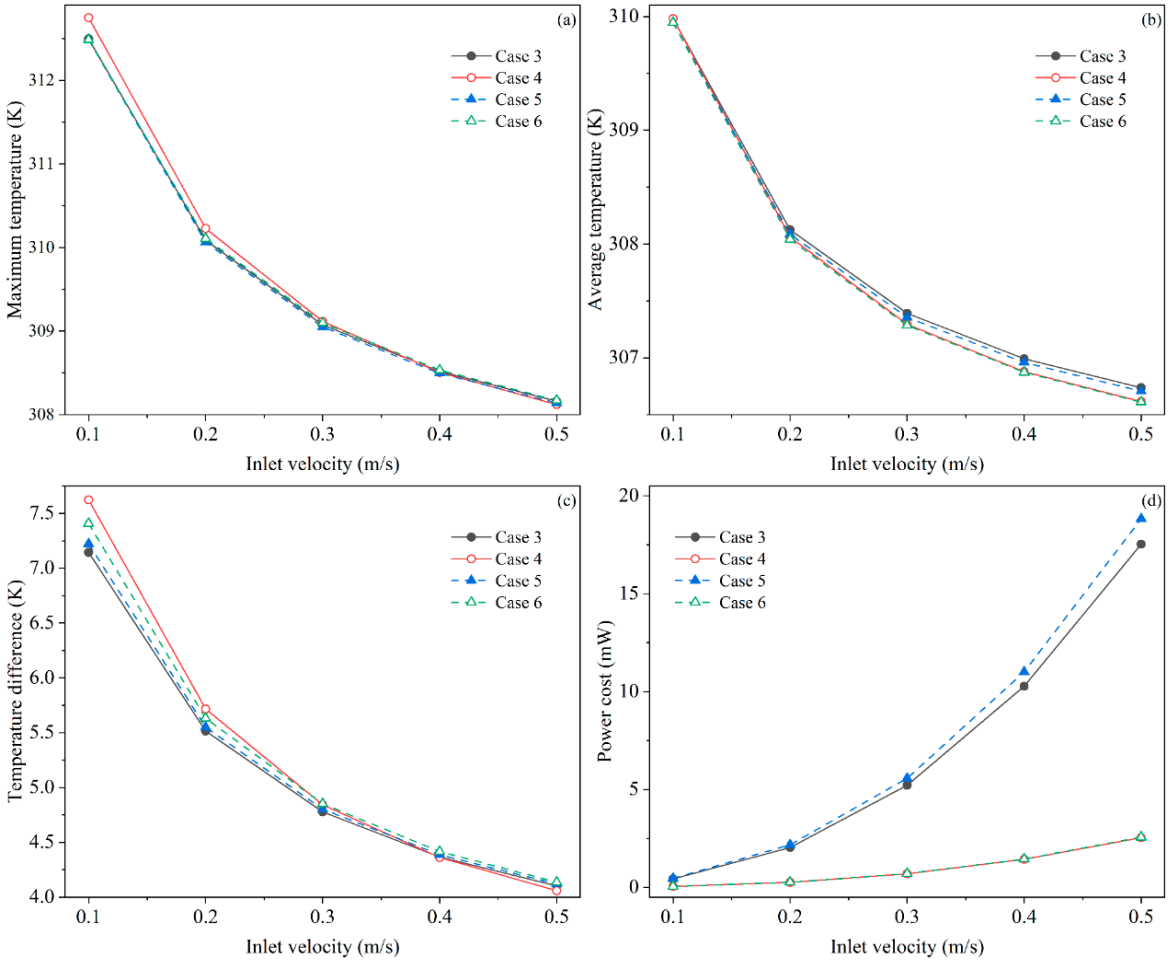

Figure 10. Thermal-hydraulic performance of Cases 3–6 with the variation of inlet flow velocity: (**a**) maximum battery temperature; (**b**) average battery temperature; (**c**) battery temperature difference, and (**d**) required power cost.

To evaluate the heat transfer performance and friction loss simultaneously for different channel designs, the non-dimensional *j/f* factor for Case 3–6 with the inlet velocity variations are demonstrated in Figure 11. Similarly, the *j/f* factors for channel designs with intersecting branches are markedly higher than those for conventional serpentine designs. At the inlet velocity of 0.2 m/s, the factor is about 0.072 and 0.069 for Cases 3 and 5, while it is 0.62 and 0.65, respectively, for Cases 4 and 6. The change of inlet and outlet distribution does not exert a great impact on straight serpentine channels, although the performance of Case 3 is slightly higher than that of Case 5. However, an evident discrepancy is observed for Cases 4 and 6. The *j/f* factor increases with the velocity growth initially and starts to decline for both cases after a certain velocity. For the flow channel design with the inlet and outlet placed on the same side, the maximum *j/f* factor of around 0.70 occurs at the velocity of 0.2 m/s while the peak value of 0.71 is realized for Case 6. Moreover, the thermal-hydraulic performance of Case 6 is higher than of Case 4, and the difference converges at the velocity of 0.3 m/s.

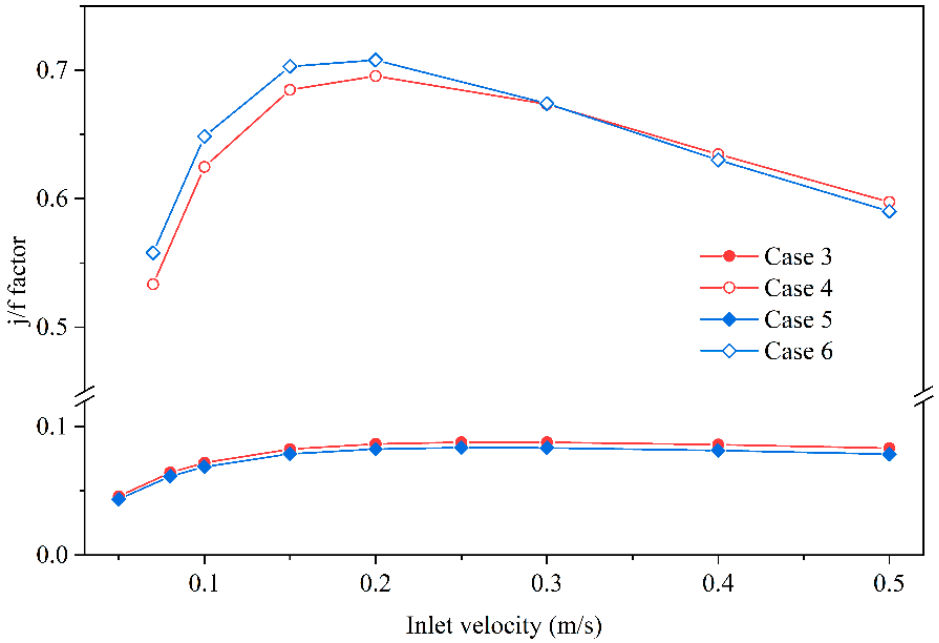

Figure 11. Variations of the *j/f* factor with the inlet velocity change for Cases 3–6.

4.3. Comparison with Existing Literature

To further illustrate the effectiveness of the intersecting channel design, the thermal–hydraulic performance achieved in present study is compared with existing literature. The *j/f* factor comparison between the present study and references [32,33] with varying mass flow rates is shown in Figure 12. It is seen that the thermal-hydraulic characteristic of the conventional serpentine design in present study is quantitatively comparable to that of the straight channel employed in reference [32], which further validates the reliability of this study. The intersected design adopted in the present study (i.e., Case-4 in Figure 11) realized the maximum *j/f* factor than other cold plate channel designs. It demonstrates that a relative superior thermal performance is obtained by the V-shaped intersected design adopted in present study at given pressure drop.

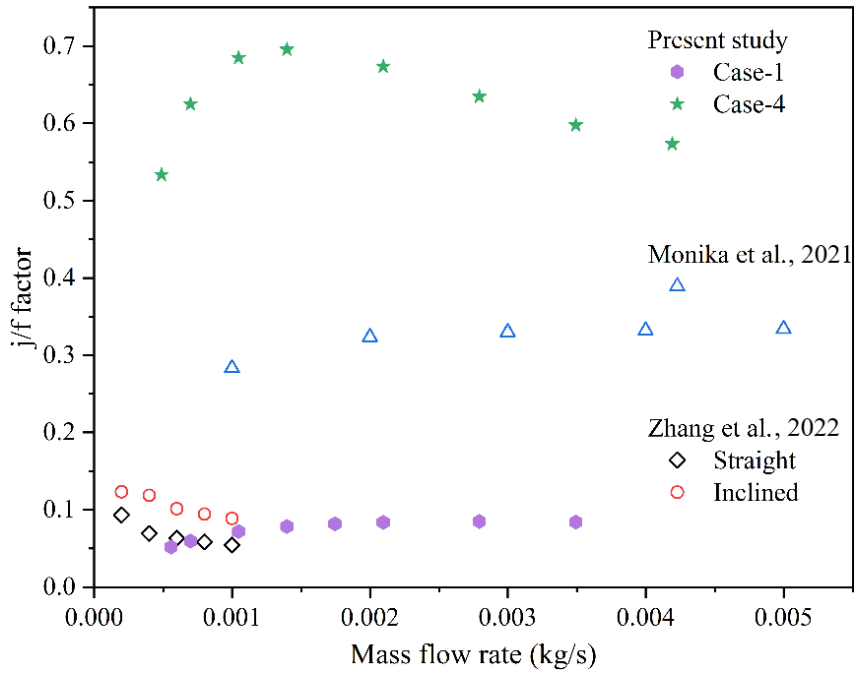

Figure 12. The *j*/*f* factor comparison with existing literature under the conditions of varying mass flow rates [32,33].

5. Conclusions

In the present study, V-shaped intersecting branches are integrated into the cold plate with serpentine flow channels to enhance the thermal performance of the liquid-based thermal management system for prismatic Li-ion batteries. Thermal-hydraulic characteristics of different channel designs are evaluated via the dimensionless j/f factor. The effects of the addition of the intersecting channel, the main flow direction, and the channel opening distribution are investigated numerically. The major conclusions drawn by the present study are summarized as follows:

(1) The addition of intersecting channels may worsen the battery temperature when the given flow velocity is low, but at high inlet velocities, the battery temperature is improved;
(2) The integrated bypass could distribute the incoming coolant into branches, thus dramatically decreasing the viscous pressure drop across the flow channel and the corresponding power consumption;
(3) The case with a widthwise flow direction reduces the battery temperature of the intersected serpentine channel case with a longitudinal flow direction for all the investigated flow velocities, although the power cost is increased slightly;
(4) Considering both the heat transfer performance and friction loss, the *j*/*f* factor is remarkably improved by the addition of intersecting channels; the change of flow direction from longitudinal to widthwise could further enhance the thermal-hydraulic characteristics for intersected designs, but for conventional serpentine channels, the longitudinal flow direction presents better performance;
(5) The inlet and outlet distributions have a negligible impact on the thermal–hydraulic performance for conventional serpentine channels, while for intersected channel designs, better performance is achieved when the inlet and outlet are distributed on the opposite sides.

Author Contributions: Conceptualization, H.L. and Y.J.; methodology, H.L. and D.N.; validation, H.L.; investigation, H.L. and X.G.; writing—original draft preparation, H.L. and X.G.; writing—review and editing, D.N., M.Y. and Y.J.; visualization, H.L. and X.G.; funding acquisition, Y.J. All authors have read and agreed to the published version of the manuscript.

Funding: This research was funded by the National Key Research and Development Program of China (Grant No. 2019YFE0116400), the National Natural Science Foundation of China (51876019), the Dalian Outstanding Scientific and Technological Talents Program (2020RJ03), and the Fundamental Research Funds for the Central Universities of China under Grant No. 3132019331 and 3132022120.

Institutional Review Board Statement: Not applicable.

Informed Consent Statement: Not applicable.

Data Availability Statement: Not applicable.

Conflicts of Interest: The authors declare no conflict of interest.

References

1. Schleussner, C.-F.; Rogelj, J.; Schaeffer, M.; Lissner, T.; Licker, R.; Fischer, E.M.; Knutti, R.; Levermann, A.; Frieler, K.; Hare, W. Science and Policy Characteristics of the Paris Agreement Temperature Goal. *Nat. Clim. Chang.* **2016**, *6*, 827–835. [CrossRef]
2. Andersen, P.H.; Mathews, J.A.; Rask, M. Integrating Private Transport into Renewable Energy Policy: The Strategy of Creating Intelligent Recharging Grids for Electric Vehicles. *Energy Policy* **2009**, *37*, 2481–2486. [CrossRef]
3. Santos, G. Road Transport and CO_2 Emissions: What Are the Challenges? *Transp. Policy* **2017**, *59*, 71–74. [CrossRef]
4. Kumar, R.R.; Alok, K. Adoption of Electric Vehicle: A Literature Review and Prospects for Sustainability. *J. Clean. Prod.* **2020**, *253*, 119911. [CrossRef]
5. Haxhiu, A.; Abdelhakim, A.; Kanerva, S.; Bogen, J. Electric Power Integration Schemes of the Hybrid Fuel Cells and Batteries-Fed Marine Vessels—An Overview. *IEEE Trans. Transp. Electrif.* **2022**, *8*, 1885–1905. [CrossRef]
6. Trends and Developments in Electric Vehicle Markets—Global EV Outlook 2021—Analysis. Available online: https://www.iea.org/reports/global-ev-outlook-2021/trends-and-developments-in-electric-vehicle-markets (accessed on 15 November 2021).
7. Zuo, H.; Zhang, B.; Huang, Z.; Wei, K.; Zhu, H.; Tan, J. Effect Analysis on SOC Values of the Power Lithium Manganate Battery during Discharging Process and Its Intelligent Estimation. *Energy* **2022**, *238*, 121854. [CrossRef]
8. Cano, Z.P.; Banham, D.; Ye, S.; Hintennach, A.; Lu, J.; Fowler, M.; Chen, Z. Batteries and Fuel Cells for Emerging Electric Vehicle Markets. *Nat. Energy* **2018**, *3*, 279–289. [CrossRef]
9. Liu, H.; Wei, Z.; He, W.; Zhao, J. Thermal Issues about Li-Ion Batteries and Recent Progress in Battery Thermal Management Systems: A Review. *Energy Convers. Manag.* **2017**, *150*, 304–330. [CrossRef]
10. Pesaran, A.A. Battery Thermal Models for Hybrid Vehicle Simulations. *J. Power Sources* **2002**, *110*, 377–382. [CrossRef]
11. Xu, B.; Lee, J.; Kwon, D.; Kong, L.; Pecht, M. Mitigation Strategies for Li-Ion Battery Thermal Runaway: A Review. *Renew. Sustain. Energy Rev.* **2021**, *150*, 111437. [CrossRef]
12. Zhao, C.; Sousa, A.C.M.; Jiang, F. Minimization of Thermal Non-Uniformity in Lithium-Ion Battery Pack Cooled by Channeled Liquid Flow. *Int. J. Heat Mass Transf.* **2019**, *129*, 660–670. [CrossRef]
13. Lin, J.; Liu, X.; Li, S.; Zhang, C.; Yang, S. A Review on Recent Progress, Challenges and Perspective of Battery Thermal Management System. *Int. J. Heat Mass Transf.* **2021**, *167*, 120834. [CrossRef]
14. Wang, Q.; Jiang, B.; Li, B.; Yan, Y. A Critical Review of Thermal Management Models and Solutions of Lithium-Ion Batteries for the Development of Pure Electric Vehicles. *Renew. Sustain. Energy Rev.* **2016**, *64*, 106–128. [CrossRef]
15. Zhao, G.; Wang, X.; Negnevitsky, M.; Zhang, H. A Review of Air-Cooling Battery Thermal Management Systems for Electric and Hybrid Electric Vehicles. *J. Power Sources* **2021**, *501*, 230001. [CrossRef]
16. Huang, Y.; Tang, Y.; Yuan, W.; Fang, G.; Yang, Y.; Zhang, X.; Wu, Y.; Yuan, Y.; Wang, C.; Li, J. Challenges and Recent Progress in Thermal Management with Heat Pipes for Lithium-Ion Power Batteries in Electric Vehicles. *Sci. China Technol. Sci.* **2021**, *64*, 919–956. [CrossRef]
17. Luo, J.; Zou, D.; Wang, Y.; Wang, S.; Huang, L. Battery Thermal Management Systems (BTMs) Based on Phase Change Material (PCM): A Comprehensive Review. *Chem. Eng. J.* **2022**, *430*, 132741. [CrossRef]
18. Subramanian, M.; Hoang, A.T.; Kalidasan, B.; Nižetić, S.; Solomon, J.M.; Balasubramanian, D.; Subramaniyan, C.; Thenmozhi, G.; Metghalchi, H.; Nguyen, X.P. A Technical Review on Composite Phase Change Material Based Secondary Assisted Battery Thermal Management System for Electric Vehicles. *J. Clean. Prod.* **2021**, *322*, 129079. [CrossRef]
19. An, Z.; Jia, L.; Ding, Y.; Dang, C.; Li, X. A Review on Lithium-Ion Power Battery Thermal Management Technologies and Thermal Safety. *J. Therm. Sci.* **2017**, *26*, 391–412. [CrossRef]
20. Saffarian, M.R.; Moravej, M.; Doranehgard, M.H. Heat Transfer Enhancement in a Flat Plate Solar Collector with Different Flow Path Shapes Using Nanofluid. *Renew. Energy* **2020**, *146*, 2316–2329. [CrossRef]
21. Sarchami, A.; Najafi, M.; Imam, A.; Houshfar, E. Experimental Study of Thermal Management System for Cylindrical Li-Ion Battery Pack Based on Nanofluid Cooling and Copper Sheath. *Int. J. Therm. Sci.* **2022**, *171*, 107244. [CrossRef]
22. Jiang, W.; Zhao, J.; Rao, Z. Thermal Performance Enhancement and Prediction of Narrow Liquid Cooling Channel for Battery Thermal Management. *Int. J. Therm. Sci.* **2022**, *171*, 107250. [CrossRef]
23. Liu, H.; Ahmad, S.; Shi, Y.; Zhao, J. A Parametric Study of a Hybrid Battery Thermal Management System That Couples PCM/Copper Foam Composite with Helical Liquid Channel Cooling. *Energy* **2021**, *231*, 120869. [CrossRef]

24. Liu, H.; Chika, E.; Zhao, J. Investigation into the Effectiveness of Nanofluids on the Mini-Channel Thermal Management for High Power Lithium Ion Battery. *Appl. Therm. Eng.* **2018**, *142*, 511–523. [CrossRef]
25. Mo, X.; Zhi, H.; Xiao, Y.; Hua, H.; He, L. Topology Optimization of Cooling Plates for Battery Thermal Management. *Int. J. Heat Mass Transf.* **2021**, *178*, 121612. [CrossRef]
26. Zuo, W.; Zhang, Y.; Jiaqiang, E.; Li, J.; Li, Q.; Zhang, G. Performance Comparison between Single S-Channel and Double S-Channel Cold Plate for Thermal Management of a Prismatic LiFePO4 Battery. *Renew. Energy* **2022**, *192*, 46–57. [CrossRef]
27. Kong, W.; Zhu, K.; Lu, X.; Jin, J.; Ni, M. Enhancement of Lithium-Ion Battery Thermal Management with the Divergent-Shaped Channel Cold Plate. *J. Energy Storage* **2021**, *42*, 103027. [CrossRef]
28. Xie, J.; Liu, X.; Zhang, G.; Yang, X. A Novel Strategy to Optimize the Liquid Cooling Plates for Battery Thermal Management by Precisely Tailoring the Internal Structure of the Flow Channels. *Int. J. Therm. Sci.* **2023**, *184*, 107877. [CrossRef]
29. Sheng, L.; Su, L.; Zhang, H.; Li, K.; Fang, Y.; Ye, W.; Fang, Y. Numerical Investigation on a Lithium Ion Battery Thermal Management Utilizing a Serpentine-Channel Liquid Cooling Plate Exchanger. *Int. J. Heat Mass Transf.* **2019**, *141*, 658–668. [CrossRef]
30. Kedam, N.; Dmitry, A.U.; Evgeniy, V.B.; Alexey, A.G. Heat Transfer Factor j and Friction Factor f Correlations for Offset Strip Fin and Wavy Fin of Compact Plate-Fin Heat-Exchangers. *Case Stud. Therm. Eng.* **2021**, *28*, 101552. [CrossRef]
31. Imran, A.A.; Mahmoud, N.S.; Jaffal, H.M. Numerical and Experimental Investigation of Heat Transfer in Liquid Cooling Serpentine Mini-Channel Heat Sink with Different New Configuration Models. *Therm. Sci. Eng. Prog.* **2018**, *6*, 128–139. [CrossRef]
32. Zhang, Y.; Zuo, W.; Jiaqiang, E.; Li, J.; Li, Q.; Sun, K.; Zhou, K.; Zhang, G. Performance Comparison between Straight Channel Cold Plate and Inclined Channel Cold Plate for Thermal Management of a Prismatic LiFePO4 Battery. *Energy* **2022**, *248*, 123637. [CrossRef]
33. Monika, K.; Chakraborty, C.; Roy, S.; Dinda, S.; Singh, S.A.; Datta, S.P. An Improved Mini-Channel Based Liquid Cooling Strategy of Prismatic LiFePO4 Batteries for Electric or Hybrid Vehicles. *J. Energy Storage* **2021**, *35*, 102301. [CrossRef]